Commun. Comput. Phys.
doi: 10.4208/cicp.120313.100713s

Vol. **15**, No. 4, pp. 1012-1028
April 2014

Local Discontinuous Galerkin Methods for the 2D Simulation of Quantum Transport Phenomena on Quantum Directional Coupler

Li Guo[1] and Yan Xu[1,*]

[1] *School of Mathematical Sciences, University of Science and Technology of China, Hefei, Anhui 230026, P.R. China.*

Received 12 March 2013; Accepted (in revised version) 10 July 2013

Available online 21 January 2014

Abstract. In this paper, we present local discontinuous Galerkin methods (LDG) to simulate an important application of the 2D stationary Schrödinger equation called quantum transport phenomena on a typical quantum directional coupler, which frequency change mainly reflects in y-direction. We present the minimal dissipation LDG (MD-LDG) method with polynomial basis functions for the 2D stationary Schrödinger equation which can describe quantum transport phenomena. We also give the MD-LDG method with polynomial basis functions in x-direction and exponential basis functions in y-direction for the 2D stationary Schrödinger equation to reduce the computational cost. The numerical results are shown to demonstrate the accuracy and capability of these methods.

AMS subject classifications: 65N30, 35Q40

Key words: Local discontinuous Galerkin method, 2D stationary Schrödinger equation, quantum transport phenomena, quantum directional coupler.

1 Introduction

Schrödinger equation is used to describe the quantum mechanical wave function in the equation of motion proposed by the Austrian physicist Schrödinger in 1926 and is considered to be the theory which is one of the fundamental theories of quantum mechanics. Schrödinger equation is widely used in atomic physics, nuclear physics and solid state physics. Solutions to Schrödinger equation can clearly describe the statistical quantum behavior of the quantum size particles in quantum systems. So how to solve Schrödinger equation becomes very important.

*Corresponding author. *Email addresses:* `lili2010@mail.ustc.edu.cn` (L. Guo), `yxu@ustc.edu.cn` (Y. Xu)

 ©2014 Global-Science Press

In this paper, we mainly discuss how to simulate numerical solutions of the 2D stationary Schrödinger equation (1.1) which can describe quantum transport phenomena

$$-\frac{1}{2}\varepsilon^2\triangle\varphi+V\varphi=E\varphi, \quad (x,y)\in\Omega, \tag{1.1}$$

where ε is the re-scaled Plank constant, E is the specified energy, $\varphi=\varphi(x,y)$ is a complex-valued function denoting the wave function, and $V=V(x,y)$ is the potential. The boundary conditions are given based on the specific issues. Many numerical methods have been developed to solve this equation. In [10, 11], the finite difference methods have been developed to simulate Schrödinger equations. Spectral method has been proposed in [8]. In [18, 19], the WKB scheme and finite element method have been used to compute this equation respectively. In addition, multi-mode approximation for resonant tunneling which can be described by the stationary Schrödinger equation is given to solve the equation in [1]. Also in [21], immersed interface method is used to compute the Schrödinger equation with discontinuous potential. In this paper, we mainly consider an important application of the 2D stationary Schrödinger equation called quantum transport phenomena on a typical quantum directional coupler shown in Fig. 1. Also various kinds of numerical methods can be found to simulate quantum transport phenomena in [4, 5, 9, 14–17, 20]. Moreover, many local discontinuous Galerkin methods have been developed to solve time dependent Schrödinger equations in [7, 12, 13, 22] but not simulate the stationary Schrödinger equation on the complicated computational domain.

We present local discontinuous Galerkin methods to solve the Schrödinger equation (1.1). Discontinuous Galerkin (DG) methods are a class of finite element methods using completely discontinuous basis functions, which are usually chosen as piecewise polynomials. The stability and convergence of LDG methods have been designed for elliptic equations in [3,6]. DG method based on non-polynomial approximation spaces has been developed in [23]. The DG method has several advantages as follows. Firstly, it can be designed as any order of accuracy. Since the order of accuracy can be locally determined in each cell, it has efficient p adaptivity. Secondly, the allowance of arbitrary triangulation even with hanging nodes makes efficient h adaptivity come true. Moreover, the method has embarrassingly high parallel efficiency because the elements only communicate with immediate neighbors regardless of the order of the accuracy of the scheme.

In this paper, we mainly develop minimal dissipation local discontinuous Galerkin (MD-LDG) method based on the basis functions of polynomials for the Schrödinger equation (1.1). In addition, we choose polynomial basis functions in x-direction and the exponential basis functions in y-direction which is typical for the simulation of quantum transport phenomena. This choice is mainly based on the change of frequency of y-direction. This method not only maintains the advantages of the general LDG methods but also saves the computational cost.

This paper is organized as follows. In Subsection 2.1, we give the model problem which we are concerned about. We give the MD-LDG method and the MD-LDG method with different basis functions in different directions for the Schrödinger equation in Sub-

sections 2.2.1 and 2.2.2 respectively. We discuss the connections and differences of these two methods in Subsection 2.2.3. In Section 3, we give the specific LDG methods for quantum transport phenomena on a typical directional coupler. Numerical results are shown in Section 4 and concluding remarks are given in Section 5.

2 The model problem and numerical methods

2.1 The model problem

Consider the 2D stationary Schrödinger equation on the domain $\Omega\subset\mathbb{R}^2$

$$-\frac{1}{2}\varepsilon^2\triangle\varphi+V\varphi=E\varphi, \quad \text{in } \Omega, \tag{2.1a}$$

$$\varphi=f, \quad \text{on } \Gamma_D, \tag{2.1b}$$

$$\frac{\partial\varphi}{\partial\boldsymbol{n}}=g, \quad \text{on } \Gamma_N, \tag{2.1c}$$

where ε is the re-scaled Plank constant, E is the specified energy, $\varphi=\varphi(x,y)$ denotes the wave function, $V=V(x,y)$ is the smooth external potential and $\boldsymbol{n}$ is the outward normal unit vector. Γ_N denotes the boundary with the Neumann boundary condition and Γ_D denotes the boundary with the Dirichlet boundary condition.

2.2 Numerical methods for the model problem

2.2.1 The MD-LDG method for the 2D stationary Schrödinger equation

In this section, we present the minimal dissipation local discontinuous Galerkin method for Eq. (2.1).

In order to define the LDG method, we rewrite Eq. (2.1) into a system of the first order equations

$$-\nabla\cdot\boldsymbol{\sigma}+\frac{2V}{\varepsilon^2}\varphi-\frac{2E}{\varepsilon^2}\varphi=0, \tag{2.2a}$$

$$\boldsymbol{\sigma}-\nabla\varphi=0, \tag{2.2b}$$

where $\boldsymbol{\sigma}=(\sigma_1,\sigma_2)$ is a vector function.

Then we introduce the finite element spaces associated to the triangulation $\Omega_h=\{K\}$ of Ω. The domain Ω can be decomposed into the set of Ω_h. we set

$$V_h=\{v\in L^2(\Omega):\ v|_K\in P^k(K),\ \forall K\in\Omega_h\},$$
$$\boldsymbol{W}_h=\{\boldsymbol{w}\in[L^2(\Omega)]^2:\ \boldsymbol{w}|_K\in[P^k(K)]^2,\ \forall K\in\Omega_h\},$$

where $P^k(K)$ denotes the set of all polynomials of degree at most k on K. For each $K\in\Omega_h$, let h_K denote the diameter of K and we set $h:=\max_{K\in\Omega_h}h_K$.

The general formulation of the LDG method for Eq. (2.1) is to find $\varphi\in V_h$ and $\boldsymbol{\sigma}\in\boldsymbol{W}_h$ such that for all $K\in\Omega_h$ and all test functions $v\in V_h$ and $\boldsymbol{w}\in\boldsymbol{W}_h$ we have

$$\int_K \boldsymbol{\sigma}\cdot\nabla v dx-\int_{\partial K}\hat{\boldsymbol{\sigma}}\cdot\boldsymbol{n}_k v ds+\frac{2}{\varepsilon^2}\int_K V\varphi v dx-\frac{2E}{\varepsilon^2}\int_K \varphi v dx=0, \tag{2.3a}$$

$$\int_K \boldsymbol{\sigma}\cdot\boldsymbol{w} dx+\int_k \varphi\nabla\cdot\boldsymbol{w} dx-\int_{\partial K}\hat{\varphi}\boldsymbol{n}_K\cdot\boldsymbol{w} ds=0, \tag{2.3b}$$

where $\boldsymbol{n}_K$ is the outward normal unit vector to the ∂K. The hat terms in the cell boundary terms in (2.3) for integration by parts for (2.2) are numerical fluxes, which are single valued functions defined on the edges and should be designed to ensure stability.

Let Γ denote the union of the boundaries of the element K of Ω_h. Γ^0 denotes the interior boundaries $\Gamma^0:=\Gamma\backslash\partial\Omega$. In order to define the fluxes, we define the average $\{q\}$ and the jump $[[q]]$ on Γ^0 of q which is a scaler. Let e be an interior edge shared by elements K_1 and K_2. Let $\boldsymbol{n}_1$ and $\boldsymbol{n}_2$ be used to denote the unit normal vectors on e pointing exterior to K_1 and K_2 respectively. And $q_i:=q|_{\partial K_i}$, we have

$$\{q\}=\frac{1}{2}(q_1+q_2),\quad [[q]]=q_1\boldsymbol{n}_1+q_2\boldsymbol{n}_2.$$

Similarly, for the vector $\boldsymbol{\tau}$ we can also define $\boldsymbol{\tau}_1$ and $\boldsymbol{\tau}_2$ as above and then we have

$$\{\boldsymbol{\tau}\}=\frac{1}{2}(\boldsymbol{\tau}_1+\boldsymbol{\tau}_2),\quad [[\boldsymbol{\tau}]]=\boldsymbol{\tau}_1\cdot\boldsymbol{n}_1+\boldsymbol{\tau}_2\cdot\boldsymbol{n}_2.$$

The fluxes are chosen as follows:

$$\begin{aligned}
&\hat{\varphi}=\varphi-\boldsymbol{\beta}\cdot[[\varphi]], && \text{on } \Gamma^0,\\
&\hat{\varphi}=f, && \text{on } \Gamma_D,\\
&\hat{\varphi}=\varphi, && \text{on } \Gamma_N,
\end{aligned}$$

and

$$\begin{aligned}
&\hat{\boldsymbol{\sigma}}=\boldsymbol{\sigma}+\boldsymbol{\beta}[[\boldsymbol{\sigma}]], && \text{on } \Gamma^0,\\
&\hat{\boldsymbol{\sigma}}=\boldsymbol{\sigma}, && \text{on } \Gamma_D\cap\Gamma^-,\\
&\hat{\boldsymbol{\sigma}}=\boldsymbol{\sigma}+\alpha(u-f)\boldsymbol{n}, && \text{on } \Gamma_D\cap\Gamma^+,\\
&\hat{\boldsymbol{\sigma}}=g\boldsymbol{n}, && \text{on}\Gamma_N,
\end{aligned}$$

where $\boldsymbol{\beta}\cdot\boldsymbol{n}_K(e)=\frac{1}{2}\text{sign}(\boldsymbol{\rho}\cdot\boldsymbol{n}_K(e))$, $\boldsymbol{\rho}$ is any nonzero piecewise constant vector, $\Gamma^-=\{e\in\Gamma:\quad \boldsymbol{\rho}\cdot\boldsymbol{n}_e<0\}$ and $\Gamma^+=\Gamma\backslash\Gamma^-$, α is chosen as $\mathcal{O}(1/h)$. The idea for the fluxes choice is following the reference [6].

2.2.2 The MD-LDG method based on non-polynomial basis functions for the 2D stationary Schrödinger equation

In this section, we are mainly interested in the frequency change which mainly reflects in y-direction for quantum transport phenomena, so here we choose the exponential basis functions in y-direction and polynomial basis functions in x-direction. For the rectangular domain, we denote the mesh by $I_{ij}=[x_{i-\frac{1}{2}},x_{i+\frac{1}{2}}]\times[y_{j-\frac{1}{2}},y_{j+\frac{1}{2}}]$. The center of the cell is $x_i=(x_{i-\frac{1}{2}}+x_{i+\frac{1}{2}})/2$, $y_j=(y_{j-\frac{1}{2}}+y_{j+\frac{1}{2}})/2$ and $\Delta x_i=x_{i-\frac{1}{2}}+x_{i+\frac{1}{2}}$, $\Delta y_j=y_{j-\frac{1}{2}}+y_{j+\frac{1}{2}}$. We make the tensor product between

$$V_{\triangle x}=\left\{1,\frac{x-x_i}{\Delta x},\left(\frac{x-x_i}{\Delta x}\right)^2,\ i=1,\cdots,nx\right\},$$

and

$$E(\alpha)=\left\{1,e^{i\alpha_j(y-y_j)},e^{-i\alpha_j(y-y_j)},\ j=1,\cdots,ny\right\},$$

where α_j is the frequency of the phenomena. The approximation space $E(\alpha)$ is actually an exponential space. In [23], the authors have proved the L^2 stability and error estimate of the DG method based on non-polynomial approximation spaces including exponential spaces for time-dependent PDEs. In [19], $E(\alpha)$ is a third order approximation space for stationary one-dimensional Schrödinger equation. And we also know $V_{\triangle x}$ has third order accuracy for PDEs. Therefore, those two basis functions by tensor product would have third order accuracy for two-dimensional PDEs.

2.2.3 Differences of the two schemes based on the different basis functions

Since these two MD-LDG methods based on polynomial basis functions and non-polynomial basis functions respectively have the same idea, we have similar scheme (2.3) and choice of the numerical fluxes for the MD-LDG scheme based on non-polynomial basis functions.

The differences between these two schemes mainly reflect in the choice of the basis functions. In the general MD-LDG method we choose polynomial basis functions while in another method we choose the exponential basis functions in y-direction and polynomial basis functions in x-direction.

Generally speaking, we choose the LDG method based on polynomial basis functions to simulate general numerical solutions. However, depending on the properties of the solution space the MD-LDG method based on non-polynomial basis functions are more efficient than the general LDG method. In this paper, we study quantum transport phenomena whose frequency change mainly reflects in y-direction. So here we not only give the general MD-LDG method based on polynomial basis functions, but also give the method with the non-polynomial basis functions that is exponential basis functions in y-direction to improve the computational efficiency.

3 Quantum transport phenomena on a typical quantum directional coupler

In this section, we give quantum transport phenomena on a typical quantum directional coupler which can be described by the 2D stationary Schrödinger equation.

3.1 The 2D stationary Schrödinger equation for the quantum transport phenomena

The 2D stationary Schrödinger equation can describe the quantum transport phenomena as follows. The domain of the 2D stationary Schrödinger equation is shown on a typical quantum directional coupler in Fig. 1. The equation is

$$-\frac{1}{2}\varepsilon^2\triangle\varphi+V\varphi=E\varphi. \tag{3.1}$$

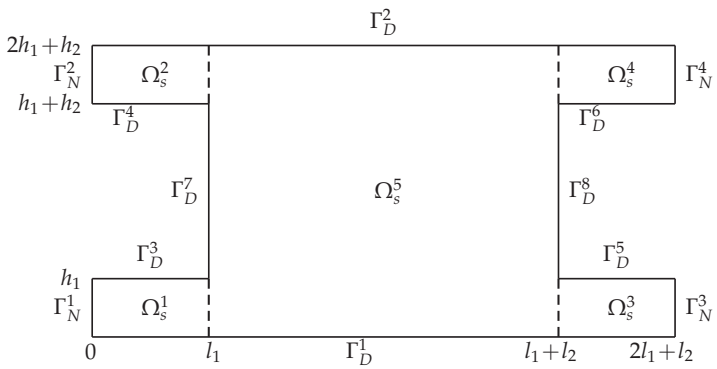

Figure 1: The computational domain.

The boundary conditions are given as follows:

- On $\Gamma_D=\bigcup_{p=1}^8\Gamma_D^p$, the confined boundary conditions are used as

$$\varphi(x,y)|_{(x,y)\in\Gamma_D}=0,$$

  which prevent electrons from leaving out of the computational domain.

- On $\Gamma_N=\bigcup_{p=1}^4\Gamma_N^p$, the transparent boundary conditions are used, which allow electrons move in and out of the computational domain. The transparent boundary conditions can be found in Appendix A for Γ_N.

3.2 The LDG method for quantum transport phenomena

In this section, we consider the rectangular meshes. The details of the LDG method for this problem are the same way as in Section 2.

First we rewrite Eq. (3.1) into a system of the first order equations

$$-(p_x+q_y)+\frac{2V}{\varepsilon^2}\varphi-\frac{2E}{\varepsilon^2}\varphi=0, \tag{3.2a}$$

$$p-\varphi_x=0, \tag{3.2b}$$

$$q-\varphi_y=0. \tag{3.2c}$$

We denote by $\varphi^+_{i+1/2,j}$ and $\varphi^-_{i+1/2,j}$ the value of φ at $x_{i+1/2}$ from the right cell, $I_{i+1,j}$, and from the left cell, $I_{i,j}$, respectively. Similarly, We denote by $\varphi^+_{i,j+1/2}$ and $\varphi^-_{i,j+1/2}$ the value of φ at $y_{j+1/2}$ from the upper cell, $I_{i,j+1}$, and from the lower cell, $I_{i,j}$, respectively. We define the complex piecewise-polynomial space $V_{\Delta x,\Delta y}$ as the space of polynomials of degree at most k in each cell I_{ij}, i.e.

$$V_{\Delta x,\Delta y}=\{v:v|_{I_{ij}}\in P^k(I_{ij}),\ i=1,\cdots,nx;\ j=1,\cdots,ny\},$$

where $P^k(I_{ij})$ be denoted to be the set of all polynomials of degree at most k in the interval I_{ij}. The finite element space V_h can be chosen as $V_h=V_{\Delta x,\Delta y}$ or $V_h=V_{\Delta x}\otimes E(\alpha)$.

The formulation of the LDG method for Eq. (3.1) is to find $\varphi,p,q\in V_h$ such that for $i=1,\cdots,nx$, $j=1,\cdots,ny$ and for all test functions $v,w,h\in V_h$, we have

$$\int_{I_{ij}} pv_x dxdy-\int_{I_j}[(\hat{p}v^-)_{i+\frac{1}{2}}-(\hat{p}v^+)_{i-\frac{1}{2}}]dy+\int_{I_{ij}} qv_y dxdy-\int_{I_i}[(\hat{q}v^-)_{j+\frac{1}{2}}-(\hat{q}v^+)_{j-\frac{1}{2}}]dx$$
$$+\frac{2}{\varepsilon^2}\int_{I_{ij}} V\varphi v dxdy-\frac{2E}{\varepsilon^2}\int_{I_{ij}}\varphi v dxdy=0, \tag{3.3a}$$

$$\int_{I_{ij}} pw dxdy+\int_{I_{ij}}\varphi w_x dxdy-\int_{I_j}[(\hat{\varphi}w^-)_{i+\frac{1}{2}}-(\hat{\varphi}w^+)_{i-\frac{1}{2}}]dy=0, \tag{3.3b}$$

$$\int_{I_{ij}} qh dxdy+\int_{I_{ij}}\varphi h_y dxdy-\int_{I_i}[(\hat{\varphi}h^-)_{j+\frac{1}{2}}-(\hat{\varphi}h^+)_{j-\frac{1}{2}}]dx=0. \tag{3.3c}$$

The hat terms in the cell boundary terms in (3.3) for integration by parts for (3.2) are numerical fluxes. The fluxes of quantum transport phenomena for the scheme (3.3) are chosen as follows:

- On the interior, the fluxes are

$$\hat{\varphi}=\varphi^+,\quad \hat{p}=p^-,\quad \hat{q}=q^-.$$

- On Γ^1_D, the fluxes are

$$\hat{\varphi}=0,\quad \hat{q}=q^+-\alpha_y(\varphi(x,0)-\varphi^+).$$

- On Γ^3_D and Γ^5_D, the fluxes are

$$\hat{\varphi}=0,\quad \hat{q}=q^-.$$

- On Γ_D^4 and Γ_D^6, the fluxes are

$$\hat{\varphi}=0, \quad \hat{q}=q^+-\alpha_y(\varphi(x,h_1+h_2)-\varphi^+).$$

- On Γ_D^2, the fluxes are

$$\hat{\varphi}=0, \quad \hat{q}=q^-.$$

- On Γ_D^7, the fluxes are

$$\hat{\varphi}=0, \quad \hat{p}=p^+-\alpha_x(\varphi(l_1,y)-\varphi^+).$$

- On Γ_D^8, the fluxes are

$$\hat{\varphi}=0, \quad \hat{p}=p^-.$$

- On Γ_N^1 and Γ_N^2, the fluxes are

$$\hat{\varphi}=\varphi^+, \quad \hat{p}=\varphi_x(0,y).$$

- On Γ_N^3 and Γ_N^4, the fluxes are

$$\hat{\varphi}=\varphi^-, \quad \hat{p}=\varphi_x(2l_1+l_2,y).$$

Here we choose $\alpha_y=\mathcal{O}(1/\Delta y)$ and $\alpha_x=\mathcal{O}(1/\Delta x)$. And the choice of the fluxes does not depend on the selection of the finite element spaces.

4 Numerical results

In this section, we present several numerical examples to illustrate the accuracy and the efficiency of the numerical schemes developed in the previous section for Eq. (2.1).

Example 4.1. We consider the 2D stationary Schrödinger equation on the domain $\Omega=[0,1]\times[0,1]$ and the boundary consists of $\Gamma_D=\{(x,0)\bigcup(x,1)|0\le x\le 1\}$ and $\Gamma_N=\{(0,y)\bigcup(1,y)|0\le y\le 1\}$. The equation is

$$-\frac{1}{2}\varepsilon^2\Delta\varphi=E\varphi, \tag{4.1a}$$

$$\varphi(x,0)=\varphi(x,1)=0, \tag{4.1b}$$

$$\varphi_x(0,y)=\mathrm{i}\sqrt{\frac{2(E-E_9)}{\varepsilon^2}}\chi_9(y), \tag{4.1c}$$

$$\varphi_x(1,y)=\mathrm{i}\sqrt{\frac{2(E-E_9)}{\varepsilon^2}}e^{\mathrm{i}\sqrt{\frac{2(E-E_9)}{\varepsilon^2}}}\chi_9(y), \tag{4.1d}$$

with the exact solution

$$\varphi(x,y)=e^{\mathrm{i}\sqrt{\frac{2(E-E_9)}{\varepsilon^2}}x}\chi_9(y), \tag{4.2}$$

where $E=0.2$, $\varepsilon=1/64$, $E_m=\frac{1}{2}m^2\pi^2\varepsilon^2$, $\chi_m(y)=\sqrt{2}\sin m\pi y$, $m=1,2,\cdots$.

The fluxes are chosen as follows:

- On the interior, the fluxes are

$$\hat{\varphi}=\varphi^+, \quad \hat{p}=p^-, \quad \hat{q}=q^-.$$

- On Γ_D, the fluxes are

$$\hat{\varphi}=0, \quad \hat{q}_{i,\frac{1}{2}}=q^+_{i,\frac{1}{2}}-\alpha_y(\varphi(x,0)-\varphi^+_{i,\frac{1}{2}}).$$

- On Γ_N, the fluxes are

$$\begin{aligned} &\hat{\varphi}_{\frac{1}{2},j}=\hat{\varphi}^+_{\frac{1}{2},j}, && \hat{p}=\varphi_x(0,y),\\ &\hat{\varphi}_{nx+\frac{1}{2},j}=\hat{\varphi}^-_{nx+\frac{1}{2},j}, && \hat{p}=\varphi_x(1,y). \end{aligned}$$

Here we choose $\alpha_y=\mathcal{O}(1/\Delta y)$ and $\alpha_x=\mathcal{O}(1/\Delta x)$.

In Table 1, we compare the CPU time by the general MD-LDG method and the MD-LDG method based on non-polynomial basis functions. We can find that the efficiency of the MD-LDG method based on non-polynomial basis functions is much higher than the general MD-LDG method to reach the same error level. Since we make full use of the properties of the solution to choose the non-polynomial basis functions we can obtain the result in Table 1. More technical details can be found in [19].

Table 1: Example 4.1, the CPU time by using different methods.

polynomials		non-polynomials	
L^2 error	CPU time	L^2 error	CPU time
9.43E-01	6.2s	6.64E-01	0.01s
1.01E-01	393s	5.45E-01	0.07s
5.84E-02	784s	2.00E-02	0.41s
6.82E-03	5003s	2.15E-03	21s

In Table 2, we give the L^2 and L^∞ error estimates and the numerical orders of accuracy for Eq. (4.1) with the exact solution (4.2) by using the general MD-LDG. We also demonstrate the L^2 and L^∞ error estimates and the numerical orders of accuracy by using the MD-LDG method based on non-polynomial basis functions with $\alpha=9\pi$ in Table 3. By comparing with two tables we can obtain that the MD-LDG method with P^k elements gives $(k+1)$-th order of accuracy and the MD-LDG method based on non-polynomial basis functions has third order accuracy. In particularly, we can see that the MD-LDG

Table 2: Example 4.1, error estimates and accuracy test for Eq. (4.1) with the exact solution (4.2) with the uniform meshes by using general LDG method.

		Real part				Imaginary part			
	Nx*Ny	L^2 error	order	L^∞ error	order	L^2 error	order	L^∞ error	order
p^2	16*16	9.43E-01	–	2.01	–	7.79E-01	–	1.88	–
	32*32	1.01E-01	3.22	3.48E-01	2.53	2.19E-02	3.91	2.03E-01	3.21
	64*64	5.33E-03	4.25	2.03E-02	4.10	2.71E-03	4.26	1.23E-02	4.04
	128*128	2.76E-04	4.27	1.20E-03	4.08	1.83E-04	3.89	7.36E-04	4.06
p^3	16*16	1.37	–	3.00	–	1.12	–	2.97	–
	32*32	3.86E-03	8.47	1.03E-02	8.19	6.29E-03	7.48	1.83E-02	7.34
	64*64	9.39E-05	5.36	2.88E-04	5.16	2.03E-04	4.96	6.52E-04	4.81

Table 3: Example 4.1, error estimates and accuracy test for the Eq. (4.1) with the exact solution (4.2) with the uniform meshes and less meshes in y-direction by using MD-LDG method based on non-polynomial basis functions with $\alpha=9\pi$.

		Real part				Imaginary part			
	Nx*Ny	L^2 error	order	L^∞ error	order	L^2 error	order	L^∞ error	order
$\alpha=9\pi$	16*4	2.00E-02	–	4.69E-02	–	8.29E-03	–	3.23E-02	–
	32*8	2.15E-03	3.21	4.35E-03	3.43	1.87E-03	2.15	3.88E-03	3.06
	64*16	2.70E-04	3.00	5.44E-04	3.00	2.68E-04	2.81	5.35E-04	2.86

scheme based on non-polynomial basis functions need less grids than the general MD-LDG method to obtain efficient results. The table also demonstrates that the MD-LDG method based on non-polynomial basis functions saves computational cost.

Example 4.2. We consider the 2D stationary Schrödinger equation (3.1) for the quantum transport phenomena on the domain shown in Fig. 1 with the following parameters

$$
\begin{aligned}
&l_1=h_1=0.2, \quad l_2=h_2=0.6, \quad E=0.6, \quad \varepsilon=0.05,\\
&V(x,y)=0, \quad (x,y)\in\Omega,\\
&a_n^r=\begin{cases}1, & n=r=1,\\ 0, & \text{else},\end{cases}\\
&E_n^r=\begin{cases}\frac{25}{2}n^2\pi^2\varepsilon^2, & r=1,2,3,4,\\ \frac{1}{2}n^2\pi^2\varepsilon^2, & r=5.\end{cases}
\end{aligned}
$$

In Table 4, we give L^1 and L^∞ error estimates for Example 4.2 where the reference solutions are obtained by using finite difference method with a uniform mesh $\Delta x=\Delta y=\frac{1}{3200}$ to show the capability and validity of the LDG method.

We give some simulation results for Example 4.2.

Table 4: Example 4.2, the L^1 and L^∞ errors of wave functions for different numerical methods with p^2 polynomials and the uniform mesh $\Delta x=\Delta y=\frac{1}{50}$ in different domains.

Domain	L^1 error	L^∞ error
Domain Ω_s^1	9.07E-05	6.52E-03
Domain Ω_s^2	5.09E-05	5.23E-03
Domain Ω_s^3	5.83E-05	4.26E-03
Domain Ω_s^4	8.23E-05	7.75E-03

- In Fig. 2, we give the numerical solutions for Eq. (3.1) with the different degree of polynomials with $\Delta x=\Delta y=\frac{1}{50}$ by using general MD-LDG method.
- In Fig. 3, we give the numerical solutions for Eq. (3.1) with the different degree of polynomials with $\Delta x=\Delta y=\frac{1}{100}$ by using general MD-LDG method.

From Figs. 2 and 3 which are obtained by using general MD-LDG method for Example 4.2, we can find that the numerical solutions for Eq. (3.1) tend to physical solutions with the degree of the polynomials increasing. Also, we can see that as the meshes increasing the simulations of Eq. (3.1) become close to the physical results. In particular, Fig. 2 shows that the numerical solution with fourth order accuracy can approximate the physical solution better by using LDG method with only 50×50 meshes. So the high order accuracy scheme can reduce the cost by decreasing the meshes.

Example 4.3. We consider the 2D stationary Schrödinger equation (3.1) for the quantum transport phenomena on the domain shown in Fig. 1 with the following parameters

$$\begin{aligned}&l_1=h_1=0.2,\quad l_2=h_2=0.6,\quad E=1.4,\quad \varepsilon=0.05,\\&V(x,y)=0,\quad (x,y)\in\Omega,\end{aligned}$$

with different coefficients of incoming waves a_n^r as follows:

- Case I

$$a_n^r=\begin{cases}1, & n=2,\ r=1,\\ 0, & \text{else.}\end{cases}$$

- Case II

$$a_n^r=\begin{cases}1, & n=2,\ r=1,\ \text{ and }\ n=1,\ r=2,\\ 0, & \text{else.}\end{cases}$$

In order to save the space, we only show the contour figures when $\Delta x=\Delta y=\frac{1}{100}$ by using the MD-LDG method based on polynomial basis functions for Example 4.3 with

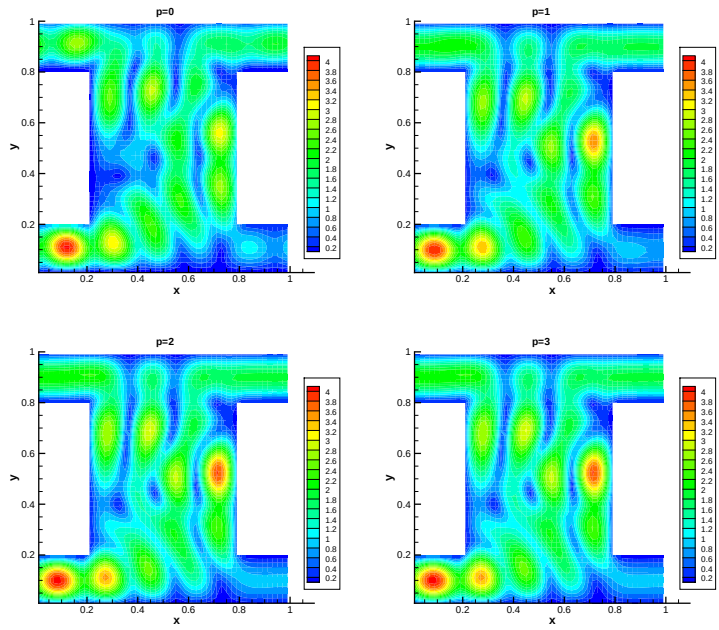

Figure 2: Example 4.2, the contour of the wave amplitude $|\varphi(x,y)|$ with the different degree of polynomials and the uniform mesh $\Delta x=\Delta y=\frac{1}{50}$ by using general MD-LDG method.

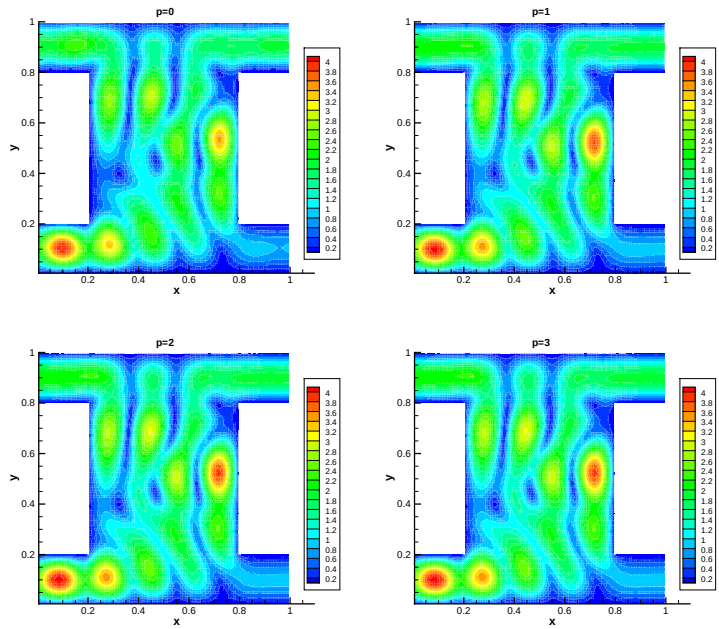

Figure 3: Example 4.2, the contour of the wave amplitude $|\varphi(x,y)|$ with the different degree of polynomials and the uniform mesh $\Delta x=\Delta y=\frac{1}{100}$ by using general MD-LDG method.

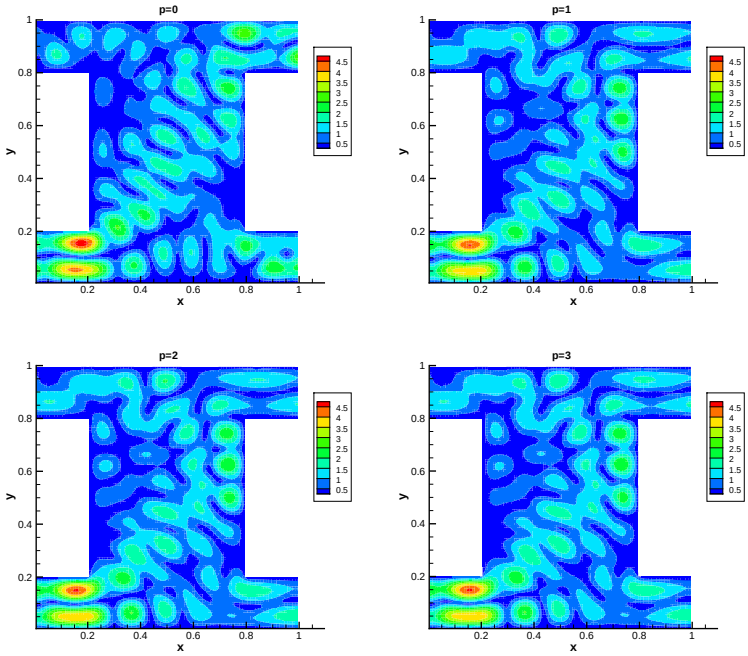

Figure 4: Example 4.3 with incoming waves Case I, the contour of the wave amplitude $|\varphi(x,y)|$ with the different degree of polynomials and the uniform mesh $\Delta x=\Delta y=\frac{1}{100}$ by using general MD-LDG method.

the incoming waves in Case I. From Fig. 4, we obtain that the numerical simulations can approximate the physical solutions.

In Fig. 5, we give the contour figures of the wave amplitude $|\varphi(x,y)|$ with two different coefficients of incoming waves. From the figure, we can see different interference phenomena.

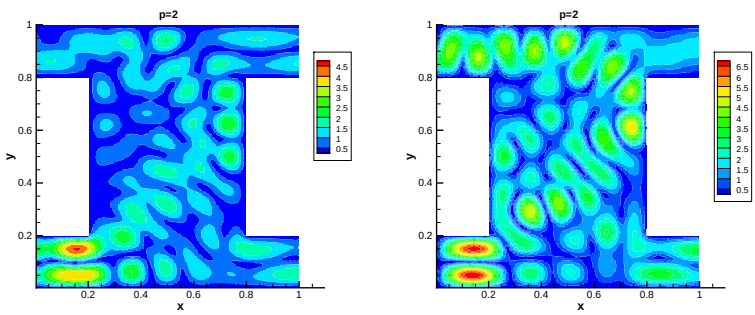

(a) Case I. (b) Case II.

Figure 5: Example 4.3, the contour of the wave amplitude $|\varphi(x,y)|$ with the different coefficients of the incoming wave a_n^r and the uniform mesh $\Delta x=\Delta y=\frac{1}{200}$ by using general MD-LDG method.

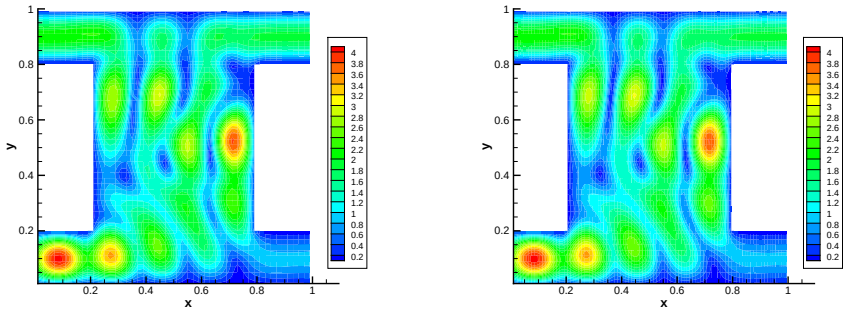

(a) For the uniform mesh $\Delta x = \Delta y = \frac{1}{50}$. (b) For the mesh $\Delta x = \frac{1}{100}, \Delta y = \frac{1}{50}$.

Figure 6: Example 4.2, the contour of the wave amplitude $|\varphi(x,y)|$ with different meshes by using MD-LDG method based on non-polynomial basis functions.

Finally, we show the figure of Example 4.2 by using MD-LDG method based on non-polynomial basis functions in Fig. 6 with different meshes.

From all the above figures, we can find that the simulation results of quantum transport phenomena are the same as in [20]. The LDG method is much easier to be extended to general potential function and more complicated computational domain.

5 Conclusion

In this paper, we have developed the minimal dissipation local discontinuous Galerkin (MD-LDG) method with piece-wise polynomial basis functions and MD-LDG method based on non-polynomial basis functions to simulate the 2D stationary Schrödinger equation. We also give the simulations of quantum transport phenomena which can be described by the 2D stationary Schrödinger equation. Numerical examples are shown to illustrate the efficiency and capability of these methods.

Acknowledgments

We thank Dr. Hao Wu from Tsinghua University for providing the related references and information to this work. Research of Y. Xu is supported by NSFC grant No. 11031007, FANEDD No. 200916, NCET No. 09-0922, Fok Ying Tung Education Foundation No. 131003.

Appendix A: The transparent boundary conditions

In this appendix, we give the transparent boundary conditions for Γ_N.

Firstly, we introduce the method of domain decomposition approach and here we consider the domain $\Omega=[0,1]\times[0,1]$ for convenience. The main idea of the subband decomposition method is to expand the wave function into series of multi-mode bases $\chi_b(x,y)$

$$\varphi(x,y)=\sum_{b=1}^{B}\phi_b(x)\chi_b(x,y),\quad \forall(x,y)\in\Omega,$$

with

$$\phi_b(x)=\langle\varphi(x,\cdot),\chi_b(x,\cdot)\rangle=\int_0^1\varphi(x,y)\overline{\chi}_b(x,y)\mathrm{d}y.$$

Let $(E_b(x),\chi_b(x,y))$ be the solutions of the eigenvalue problem

$$-\frac{1}{2}\varepsilon^2\partial_{yy}\chi_b(x,y)+V(x,y)\chi_b(x,y)=E_b(x)\chi_b(x,y),$$

with

$$\langle\chi_b(x,\cdot),\chi_{b'}(x,\cdot)\rangle=\delta_{b,b'},$$

and the boundary conditions are determined by the boundary conditions of the wave function on $y-$direction. Then we have the coupled Schrödinger system for $\phi_b(x)$

$$-\frac{1}{2}\varepsilon^2\partial_{xx}\phi_b-\varepsilon^2\sum_{b'=1}^{B}c^1_{bb'}\partial_x\phi_{b'}-\frac{1}{2}\varepsilon^2\sum_{b'=1}^{B}c^2_{bb'}\phi_{b'}=(E-E_b)\phi_b, \tag{A.1}$$

where

$$c^1_{bb'}(x)=\int_0^1\overline{\chi}_b(x,y)\partial_x\chi_{b'}(x,y)\mathrm{d}y,$$
$$c^2_{bb'}(x)=\int_0^1\overline{\chi}_b(x,y)\partial_{xx}\chi_{b'}(x,y)\mathrm{d}y.$$

It is easy to check that

$$c^1_{bb}(x)=c^2_{bb}(x)=0.$$

Eq. (A.1) can be discretized in the central difference form

$$-\frac{\varepsilon^2}{2h^2}\left(\phi_b^{n+1}-2\phi_b^n+\phi_b^{n-1}\right)-\frac{\varepsilon^2}{2h}\sum_{b'}c^{1n}_{bb'}\left(\phi_{b'}^{n+1}-\phi_{b'}^{n-1}\right)-\frac{\varepsilon^2}{2}\sum_{b'}c^{2n}_{bb'}\phi^n_{b'}=(E-E^n_b)\phi^n_b, \tag{A.2}$$

with $\phi^n_b=\phi_b(x_n)$, $E^n_b=E_b(x_n)$ and $c^{in}_{bb'}=c^i_{bb'}(x_n)$ $(i=1,2)$.

Secondly, we give the transparent condition for (3.1). The detailed derivations can be found in [2,20].

- For $r=1,2$, the boundary condition on Γ_N^r is

$$\varepsilon\partial_x\varphi(0,y)=\sum_{E>E_n^r}\mathrm{i}\sqrt{2(E-E_n^r)}(2a_n^r-\phi_n^r(0))\chi_n^r(0,y)$$
$$+\sum_{E\le E_n^r}\sqrt{2(E_n^r-E)}\phi_n^p(0)\chi_n^r(0,y),\quad \forall(0,y)\in\Gamma_N^r.$$

- For $r=3,4$, the boundary condition on Γ_N^r is

$$\varepsilon\partial_x\varphi(2l_1+l_2,y)=\sum_{E>E_n^r}\mathrm{i}\sqrt{2(E-E_n^r)}(\phi_n^r(2l_1+l_2)-2a_n^r)\chi_n^r(2l_1+l_2,y)$$
$$-\sum_{E\le E_n^r}\sqrt{2(E_n^r-E)}\phi_n^r(2l_1+l_2)\chi_n^r(2l_1+l_2,y),\quad \forall(2l_1+l_2,y)\in\Gamma_N^r.$$

Here a_n^r are the coefficients of the incoming waves.

References

[1] N. Ben Abdallah and H. Wu, A generalized stationary algorithm for resonant tunneling: multi-mode approximation and high dimension, Communications in Computational Physics, 10(2011), no. 4, 882-898.

[2] X. Antoine, C. Besse, M. Ehrhardt and A. Schädle, A review of transparent and artificial boundary conditions techniques for linear and nonlinear Schrödinger equations, Communications in Computational Physics, 4(2008), no. 4, 729-796.

[3] D.N. Arnold, F. Brezzi, B. Cockburn and L.D. Marini, Unified analysis of discontinuous Galerkin methods for elliptic problems, SIAM Journal on Scientific Computing, 39(2002), no. 5, 1749-1779.

[4] W.Z. Bao, S. Jin and P.A. Markowich, On time-splitting spectral approximations for the Schrödinger equation in the semiclassical regime, Journal of Computational Physics, 175(2002), 487-524.

[5] W.Z. Bao, S. Jin and P.A. Markowich, Numerical studies of time-splitting spectral discretizations of nonlinear Schrödinger equations in the semiclassical regime, SIAM Journal on Scientific Computing, 25(2003), no. 1, 27-64.

[6] B. Cockburn and B. Dong, An analysis of the minimal dissipation local discontinuous Galerkin method for convection-diffusion problems, Journal of Scientific Computing, 32(2007), no. 2, 233-262.

[7] K. Fan, W. Cai and X. Ji, A generalized discontinuous Galerkin (GDG) method for Schrödinger equations with nonsmooth solutions, Journal of Computational Physics, 227(2008), no. 4, 2387-2410.

[8] J. Gagelman and H. Yserentant, A spectral method for Schrödinger equations with smooth confinement potentials, Numerische Mathematik, 122(2012), no. 2, 383-398.

[9] H.Y. Jiang, S.H. Shao, W. Cai and P.W. Zhang, Boundary treatments in non-equilibrium Green's function (NEGF) methods for quantum transport in nano-MOSFETs, Journal of Computational Physics, 227(2008), no. 13, 6553-6573.

[10] L.H. Kong, Y.L. Duan, L. Wang, X.L. Yin and Y.P. Ma, Spectral-like resolution compact ADI finite difference method for the multi-dimensional Schrödinger equations, Mathmatical and Computer Modelling, 55(2012), no. 5-6, 1798-1812.
[11] X. Li, L.M. Zhang and S.S. Wang, A compact finite difference scheme for the nonlinear Schrödinger equation with wave operator, Applied Mathematics and Computation, 219(2012), no. 6, 3187-3197.
[12] T. Lu and W. Cai, A Fourier spectral-discontinuous Galerkin method for time-dependent 3-D Schröinger-Poisson equations with discontinuous potentials, Journal of Computational and Applied Mathematics, 220(2008), no. 1-2, 588-614.
[13] T. Lu, W. Cai and P.W. Zhang, Conservative local discontinuous Galerkin methods for time dependent Schrödinger equation, International Journal of Numerical Analysis and Modeling, 2(2005), no. 1, 75-84.
[14] P.A. Markowich, P. Pietra and C. Pohl, Numerical approximation of quadratic obaservables of Schrödinger-type equations in the semiclassical limit, Numerische Mathematik, 81(1999), no. 4, 595-630.
[15] P.A. Markowich, P. Pietra, C. Pohl and H.P. Stimming, A wigner-measure analysis of the Dufort-Frankel scheme for the Schrödinger equation, SIAM Journal on Numerical Analysis, 40(2002), no. 4, 1281-1310.
[16] E. Polizzi and N. Ben Abdallah, Subband decomposition approach for the simulation of quantum electron transport in nanostructures, Journal of Computational Physics, 202(2005), 150-180.
[17] S.H. Shao, T. Lu and W. Cai, Adaptive conservative cell average spectral element methods for transient Wigner equation in quantum transport, Communications in Computational Physics, 10(2011), no. 4, 882-898.
[18] A. Soba, A finite element method solver for time-dependent and stationary Schrödinger equations with a generic potential, Communications in Computational Physics, 9(2011), no. 3, 711-739.
[19] W. Wang and C.W. Shu, The WKB local discontinuous Galerkin method for the simulation of Schrödinger equation in a resonant tunneling Diode, Journal of Scientific Computing, 40(2009), 360-374.
[20] H. Wu, Domain and subband decomposition approach for the 2D simulation of quantum transport phenomena, preprint.
[21] H. Wu, High order scheme for Schrödinger equation with discontinuous potential I: immersed interface method, Numerical Mathematics: Theory, Methods and Applications, 4(2011), no. 4, 576-597.
[22] Y. Xu and C.W. Shu, Local discontinuous Galerkin methods for nonlinear Schrödinger equations, Journal of Computational Physics, 205(2005), no. 1, 72-97.
[23] L. Yuan and C.W. Shu, Discontinuous Galerkin method based on non-polynomial approximation spaces, Journal of Computational Physics, 218(2006), no. 1, 295-323.